Proton-Transfer Dynamics in the Activation of Cytochrome P450eryF

Victor Guallar,*,† Danni L. Harris,‡ Victor S. Batista,† and William H. Miller*,†

Contribution from the Department of Chemistry, University of California, and Chemical Sciences Division, Lawrence Berkeley National Laboratory, Berkeley, California 94720, and Molecular Research Institute, 2495 Old Middlefield Way, Mountain View, California 94043

Received June 21, 2001

Abstract: Molecular dynamics simulations are combined with quantum chemistry calculations of instantaneous proton-transfer energy profiles to investigate proton-transfer events in the transient pathway of cytochrome P450eryF (6-deoxyerythronolide B hydroxylase; CYP107A1), from the oxyferrous species to the catalytically active ferryl oxygen species (compound I). This reaction is one of the most fundamental unresolved aspects in the mechanism of oxidation that is common to all cytochrome P450s. We find that this process involves an ultrafast proton transfer from the crystallographic water molecule W519 to the distal oxygen bound to the heme group, and a subsequent proton-transfer event from W564 to W519. Both proton-transfer events are found to be endothermic in the oxyferrous state, suggesting that the oxyferrous reduction is mechanistically linked to the proton-transfer dynamics. These findings indicate that the hydrogen bond network, proximate to the O_2-binding cleft, plays a crucial functional role in the enzymatic activation of P450s. Our results are consistent with the effect of mutations on the enzymatic efficacy.

I. Introduction

Cytochrome P450eryF (CYP107A1) is a member of the ubiquitous family of cytochrome P450s. These heme proteins, with over 500 known isozymes,[1,2] catalyze the monoxygenation of a diverse set of substrates involved in carcinogenesis and drug metabolism.[3-5] Experimental[6,7] and theoretical[8] studies suggest that P450 enzymes catalyze monoxygenation reactions by transfer of a single oxygen atom from a ferryl oxygen adduct (Fe═O) of the heme unit (compound I).[6,7] Formation of the oxidative intermediate involves a catalytic cycle that is common to all P450 enzymes. This cycle is presented in Figure 1.

In the first step of the cycle, the substrate binds to the ferric resting form, displacing water molecules that are coordinated to the heme iron at the binding site. Next, a one-electron reduction results in substrate-bound ferrous heme species. Molecular oxygen binds to the heme iron, forming the last metastable intermediate. The subsequent steps occur extremely rapidly, making a definite characterization of the transient intermediates a rather difficult task. In particular, the transient pathway of cytochrome P450eryF from the oxyferrous species to the catalytically active ferryl oxygen species is one of the most fundamental unresolved aspects of this cycle. The goal of this paper is to address this fundamental step.

Experimental and computational work[8-11] suggests that the cycle involves a second one-electron reduction of the oxyferrous species. This reaction forms the twice-reduced dioxygen species that quickly reacts with two protons to produce compound I and water. This model is also consistent with cryogenic crystal structure studies of the oxyferrous P450cam species,[7] showing evidence of an additional water molecule, not present in the ferric substrate-bound crystal structure. Compound I has been investigated in terms of spectroscopic[6] and cryogenic crystallographic studies.[7] Its electronic structure and unpaired spin distribution have also been examined.[8,12-15] Compound I is the catalytically active species that oxidizes substrates, forming products and returning to the ferric resting state of the enzyme. These subsequent steps in the catalytic cycle model are consistent with isotopically enriched molecular oxygen experiments.[16-18] These studies show that the "proximal" oxygen,

(1) Nelson, D. *Arch. Biochem. Biophys.* **1999**, *369*, 1.
(2) Nelson, D.; Koymans, L.; Kamataki, T.; Stegeman, J.; Feyereisen, R.; Waxman, D.; Waterman, M.; Gotoh, O.; Coon, M.; Estabrook, R.; Gunsalus, I.; Nebert, D. *Pharmacogenetics* **1996**, *6*, 1.
(3) Hayaishi, O. In *Molecular Mechanisms of Oxygen Activation*; Academic Press: New York, 1974.
(4) Keevil, T.; Mason, H. *Methods Enzymol.* **1978**, *52*, 2.
(5) Malstrom, B. *Annu. Rev. Biochem.* **1982**, *51*, 21.
(6) Egawa, T.; Shimada, H.; Ishimura, Y. *Biochem. Biophys. Res. Commun.* **1994**, *201*, 1464.
(7) Schlichting, I.; Berendzen, J.; Chu, K.; Stock, A.; Maves, S.; Benson, D.; Sweet, R.; Ringe, D.; Petsko, G.; Sligar, S. *Science* **1994**, *287*, 1615.
(8) Harris, D.; Loew, G.; Waskell, L. *J. Inorg. Biochem.* **2001**, *83*, 309.

(9) Davydov, R.; Kappl, R.; Huttermann, J.; Peterson, J. *FEBS Lett.* **1991**, *295*, 113.
(10) Benson, D.; Suslick, K.; Sligar, S. *Biochemistry* **1997**, *36*, 5104.
(11) Aikens, J.; Sligar, S. *J. Am. Chem. Soc.* **1994**, *116*, 1143.
(12) Ogliaro, F.; Cohen, S.; deVisser, S.; Shaik, S. *J. Am. Chem. Soc.* **2000**, *122*, 12892.
(13) Filatov, M.; Harris, N.; Shaik, S. *J. Chem. Soc., Perkin Trans.* **1999**, *2*, 399.
(14) Green, M. *J. Am. Chem. Soc.* **1999**, *121*, 7939.
(15) Harris, D.; Loew, G. *J. Am. Chem. Soc.* **1998**, *120*, 8941.
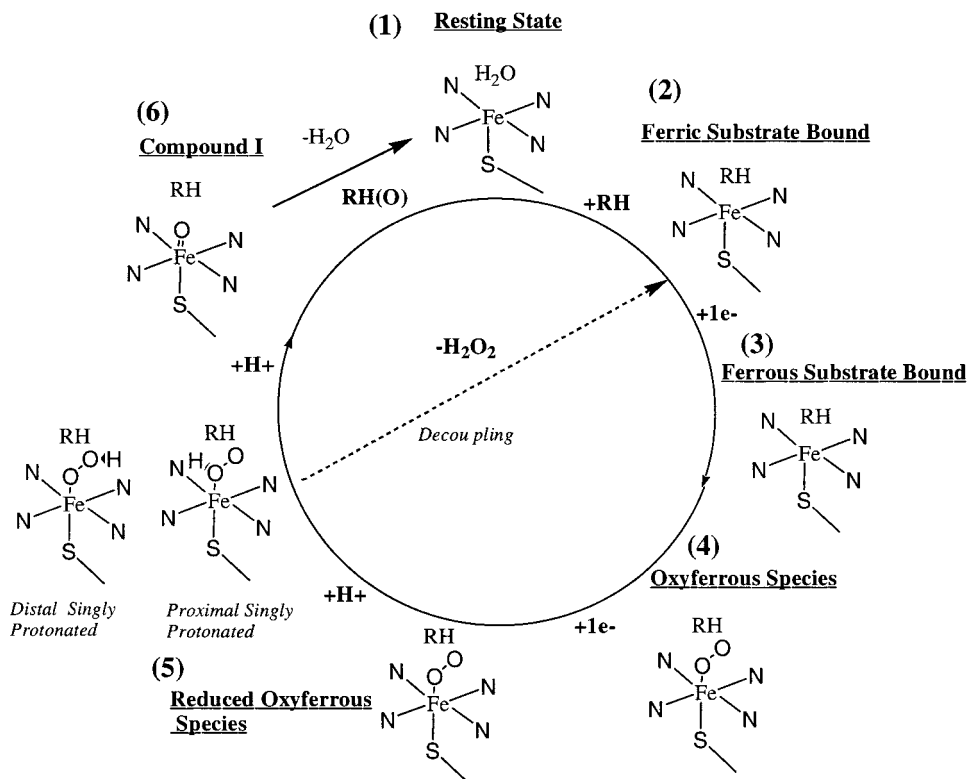(16) Jones, P.; Rettie, A.; Trager, W. *J. Med. Chem.* **1990**, *33*, 1242.

Figure 1. Enzymatic cycle of CYP450s showing the role of proton additions to the reduced oxyferrous species in the formation of compound I.
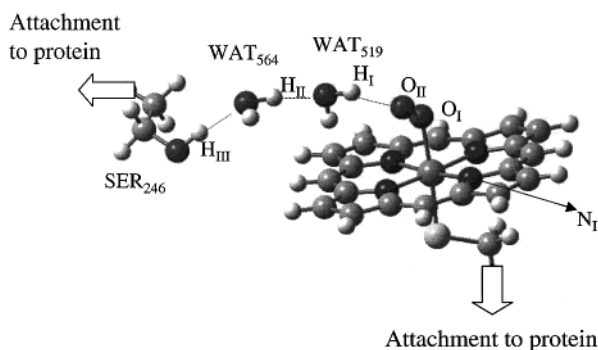

Figure 2. A portion of the substrate-binding site in the vicinity of the O_2-binding cleft. An ordered internal hydrogen bond network is shown including the heme-bound O_2 via W519 and W564 and Ser246.

directly bound to the heme iron, is the one transferred to substrates via compound I, while the other "distal" oxygen is involved in the concurrent formation of water.

Figure 2 shows the environment of the oxygen-binding cleft of P450eryF, in accord with the crystallographic coordinates of the ferric heme substrate-bound form.[19] This crystal structure has been used as the initial configuration in molecular dynamics (MD) simulations.[20] These computational studies showed that the distal oxygen atom, in the dioxygen ligand, has two dynamically stable hydrogen bonds. One of these hydrogen bonds is formed with the substrate (not shown in Figure 1), and the other one is formed with W519 (H-bond 1). These early MD simulations also found clear evidence for a dynamically stable network of hydrogen bonds that connects W519 to W564

(H-bond 2), and W564 to Ser246 (H− bond 3). Surprisingly, the feasibility of proton transfer through this extended network of hydrogen bonds has never been investigated. In this paper we investigate this fundamental aspect.

Rigorous computer simulations of proton transfer are particularly challenging, because the description of proton motion requires that one include quantum mechanical effects such as zero-point motion, tunneling, and the interference phenomena. A number of mixed quantum−classical methods have been developed and applied to simulations of proton transfer.[21−39] Most of these methods, however, describe the coupling between light and heavy particle degrees of freedom only approximately, according to branching processes defined by stochastic hops that collapse, transferring protons into either of the possible states of distinct character. Other methods are applicable only to single proton-transfer reactions, or model light and heavy

(17) Sligar, S.; Murray, R. In *Cytochrome P450cam and Other Bacterial P-450 Enzymes*; Plenum Press: New York, 1986.
(18) Atkins, W.; Sligar, S. *J. Am. Chem. Soc.* **1905**, *27*, 1610.
(19) Cupp-Vickery, J.; Poulos, T. *Nat. Struct. Biol.* **1995**, *2*, 144.
(20) Harris, D.; Loew, G. *J. Am. Chem. Soc.* **1996**, *118*, 6377.

(21) Morillo, M.; Cukier, R. I. *J. Phys. Chem.* **1990**, *92*, 4833.
(22) Suarez, A.; Silbey, R. *J. Chem. Phys.* **1991**, *94*, 4809.
(23) Aqvist, J.; Warshel, A. *Chem. Rev.* **1993**, *93*, 2523.
(24) Liu, D. G. T. Y.; Schenter, G.; Garrett, B. C. *J. Phys. Chem.* **1994**, *98*, 8396.
(25) Borgis, D.; Tarjus, G.; Azzuoz, H. *J. Phys. Chem.* **1992**, *96*, 3188.
(26) Borgis, D.; Tarjus, G.; Azzuoz, H. *J. Phys. Chem.* **1992**, *97*, 1390.
(27) Laria, D.; Ciccoti, G.; Ferrario, M.; Kapral, R. *J. Chem. Phys.* **1992**, *97*, 378.
(28) Fedorowicz, A.; Mavri, J.; Bala, P.; Koll, A. *Chem. Phys. Lett.* **1998**, *289*, 457.
(29) Koper, M. T. M.; Voth, G. A. *Chem. Phys. Lett.* **1998**, *282*, 100.
(30) Boroda, Y. G.; Calhoun, A.; Voth, G. A. *J. Chem. Phys.* **1997**, *107*, 8940.
(31) Guo, Y.; Wilson, A.; Chabalowski, C. F.; Thompson, D. L. *J. Chem. Phys.* **1998**, *109*, 9258.
(32) Guo, Y.; Li, S.; Thompson, D. L. *J. Chem. Phys.* **1997**, *107*, 2853.
(33) Warshel, A.; Chu, Z. *J. Chem. Phys.* **1990**, *93*, 4003.
(34) Lobaugh, J.; Voth, G. A. *J. Chem. Phys.* **1996**, *104*, 2056.
(35) Lobaugh, J.; Voth, G. A. *J. Chem. Phys.* **1997**, *106*, 2400.
(36) Brewer, M.; Schmitt, U.; Voth, G. A. *Biophysics* **2001**, *80*, 1691.
(37) Day, T. J. F.; Schmitt, U.; Voth, G. A. *J. Am. Chem. Soc.* **2000**, *122*, 12027.
(38) Warshel, A.; Jen, C. Y.; Villa, J. *Biophys. J.* **2001**, *114* (Part 2) and references therein.
(39) Tu, C.; Tripp, B. C.; Ferry, J. G.; Silverman, D. N. *J. Am. Chem. Soc.* **2001**, *123*, 5861.

degrees of freedom on different "dynamical footing"—i.e., these methods require that one specify a priori the "quantum" or "classical" nature of each degree of freedom in the system and integrate their equations of motion only approximately according to a self-consistent propagation scheme. In recent work,[40,41] rigorous semiclassical methods have been developed to simulate proton-transfer dynamics as coupled to low- and high-frequency reorganization coordinates. These methods integrate the equations of motion for all degrees of freedom on the same dynamical footing and have the distinct advantage that they do not require one to specify the quantum or classical nature of the degrees of freedom in the system.

In this paper, however, we adopt a simple procedure appropriate to solve the problem of interest. The goal is to establish the conditions under which direct protonation of the heme-bound distal oxygen occurs via proton transfer from adjacent proton donors. This is accomplished simply by finding optimal configurations for proton transfer and analyzing the probability of proton transfer, assuming a frozen nuclear configuration for all other degrees of freedom. This approximation is subsequently validated in terms of the comparison of the lifetime of optimal configurations for proton transfer and the time scales for proton translocation. The results obtained with this approximate method show the first direct evidence of an ultrafast proton-transfer mechanism in P450s. These theoretical findings provide an explanation for the experimental fact that enzymatic dysfunction is correlated with configurational disorder of water molecules in the O_2-binding cleft.

Classical molecular dynamics simulations of the complete enzyme are combined with calculations of instantaneous proton-transfer energy profiles, obtained according to the ab initio nonlocal density functional theory (DFT). An exhaustive DFT quantum chemical characterization of the hydrogen bond network is presented. The role of the extended hydrogen bond network in the stabilization of the proton-transfer product is investigated. The nature of the mechanistic coupling between electronic reduction and proton transfer is investigated by exploring proton transfer in the oxyferrous and reduced oxyferrous forms. Our calculations show, for the first time, that the electric field associated with the twice-reduced dioxygen species is sufficiently strong as to promote proton transfer from W519 to the distal oxygen. However, this process occurs only when it is assisted by the hydrogen bond network proximate to the O_2-binding cleft (see Figure 1). The initial proton-transfer event breaks H-bond 1 and induces a conformational relaxation of the extended hydrogen bond network. This process brings W519 closer to W564 and promotes a second proton transfer from W564 to W519. This double proton-transfer mechanism, where W519 plays a central role, is consistent with mutation experiments. It was found that mutations that affect the occupancy and/or mobility of the W519 correlate with reduction in enzymatic turnover for the enzyme[42,43]

The paper is organized as follows. Section 2 describes the methods implemented to analyze the structure and dynamics of the hydrogen bond network in the O_2-binding cleft of

P450eryF. Section 3 presents our results. Finally, section 4 summarizes and concludes.

II. Methods

Section II.A describes the molecular dynamics approach implemented to sample a thermally equilibrated ensemble of reactant configurations. Section II.B describes the electronic structure calculations of proton-transfer energy profiles. Finally, section II.C describes the methods implemented to estimate the proton-transfer probability and the times scales for proton transfer.

A. Molecular Dynamics Approach. The P450eryf crystallographic structure[19] is solvated with a 6 Å layer of water molecules (i.e., a total of 15 000 atoms). The ligand O_2 is added to the heme iron, and the total system is parametrized according to ref 20. The water molecules are equilibrated at 300 K for 40 ps, using the SANDER module of AMBER 5.[44] The complete model of the solvated enzyme, in its reduced oxyferrous bound heme form, is equilibrated by harmonically constraining the crystal structure coordinates using a force constant of 10.0 kcal/Å. The harmonic constraints are subsequently decreased over 5 ps time intervals from 10 kcal/$Å^2$ mol to 5, 1, 0.5, and 0.1 kcal/$Å^2$. The final configuration is used to generate five statistically independent configurations by propagating the system for another 10 ps, after reinitializing velocities. During this final equilibration process, the outermost shell of solvating water molecules is harmonically constrained with a 0.1 kcal/$Å^2$ force constant in the oxygen atoms. We have compared our simulations with calculations where we have included the Ewald summation with periodic boundary conditions, and we have not noticed any significant changes with respect to the results obtained with the solvation-shell approximation described above.

An ensemble of reactant configurations is generated by propagating each statistically independent final configuration for another 500 fs. A configuration is sampled every 9.5 fs—i.e., approximately the vibrational period of the O(W519)−H_I coordinate (3500 cm^{-1} frequency mode). This method is necessary to overcome the constraints on the O−H distances imposed by the SHAKE algorithm during the equilibration procedure. This procedure also serves as an unbiased random search of optimal configuration for proton transfer. These configurations are subsequently examined in terms of quantum chemistry DFT calculations. It is found that optimal configurations correspond in general to classical turning points in proton motion and to a protein environment that stabilizes the product configuration. Reactive configurations are therefore thermally populated according to the dynamics of vibrational energy redistribution in the entire system, and they are not necessarily constrained to small-amplitude fluctuations around a minimum energy path (MEP).

B. Electronic Structure Calculations. The model of the P450 heme site used in all quantum chemistry calculations is an iron−porphyrin complex with no porphyrin substituents and a methyl mercaptide (SCH_3^-) axial ligand for the heme iron. This model was implemented for computing the proton-transfer energy profiles in three different model systems for the hydrogen bond network, proximate to the O_2-binding cleft, as described in section III.A. All electronic structure calculations are performed at the nonlocal unrestricted DFT level of theory using the hybrid B3LYP functional with the suite of programs Q-Chem 2.0[45] and a generic double-ζ basis set: O, 6-31G$*$+; N, 3-21G$*$; C, 3-21G$*$; Fe, 6-31G$*$; S, 3-21G$*$; H, 3-21G$*$. The hybrid functional B3LYP has been validated in small molecular systems[46] by

(40) Guallar, V.; Batista, V.; Miller, W. *J. Chem. Phys.* **2000**, *113*, 9510.
(41) Guallar, V.; Batista, V. S.; Miller, W. H. *J. Chem. Phys.* **1999**, *110*, 9922.
(42) Cupp-Vickery, J.; Han, O.; Hutchinson, C. R.; Poulos, T. L. *Nat. Struct. Biol.* **1996**, *3*, 632.
(43) Cupp-Vickery, J. R.; Poulos, T. *Steroids* **1997**, *62*, 112.

(44) Case, D.; Pearlman, D.; Caldwell, J.; Cheatham, T.; Ross, W.; Simmerling, C.; Darden, T.; Merz, K.; Stanton, R.; Chen, A.; Vincent, J.; Crowley, M.; Tsui, V.; Radmer, R.; Duan, Y.; Pitera, J.; Massova, I.; Kollman, P. *Amber 5.0*, University of California, 1997.
(45) Kong, J.; White, C.; Krylov, A. I.; Sherrill, C.; Adamson, R.; Furlani, T.; Lee, M.; Lee, A.; Gwaltney, S.; Adams, T.; Ochsenfeld, C.; Gilbert, A.; Kedziora, G.; Rassolov, V.; Maurice, D.; Nair, N.; Shao, Y.; Besley, N.; Maslen, P.; Dombroski, J.; Daschel, H.; Zhang, W.; Korambath, P.; Baker, J.; Byrd, E.; Voorhis, T. V.; Oumi, M.; Hirata, S.; Hsu, C.-P.; Ishikawa, N.; Florian, J.; Warshel, A.; Johnson, B.; Gill, P.; Head-Gordon, M.; Pople, J. *J. Comput. Chem.* **2000**, *21*, 1532.

comparing the proton-transfer energy barriers and the overall nature of the proton-transfer energy surfaces with the corresponding results obtained with high-level coupled cluster methods. We have also verified that our ab initio calculations reproduced the geometries and relative energies obtained with a larger basis set, e.g., by using lacv3p** (for the Fe atom), cc-pvtz(-f) (for N, S, O, and H atoms involved in H-bonding), and 6-31G* (for the remaining C and H atoms).

C. Proton-Transfer Analysis. Proton-transfer dynamics is described by simulating the dynamics of the thermally equilibrated solvated enzyme in the reduced oxyferrous heme form. Nuclear configurations are sampled throughout the evolution of the system, and the instantaneous probability of proton transfer is estimated assuming that the motion of the remaining degrees of freedom is much slower than the proton motion. This approximation allows us to simulate proton transfer according to a full quantum dynamics simulation through a one-dimensional proton-transfer energy profile. The survival probability, $P(t)$, can be computed in each sampled configuration by propagating the wave packet that describes the proton motion, according to the split operator method.[47] The survival probability $P(t)$ is defined as the probability that at time t the system is still on the reactant side of the dividing surface (in coordinate space) that separates reactants and products,

$$P(t) \equiv \langle \Psi_0 | \, e^{i\hat{H}t/\hbar} h(\mathbf{q}) \, e^{-i\hat{H}t/\hbar} \, | \Psi_0 \rangle \qquad (2.1)$$

Here, $\hat{H}$ is the Hamiltonian operator of the molecular system, $\mathbf{q}$ represents the mass-weighted nuclear coordinates, and $h(\mathbf{q})$ is a function of the proton coordinates that is 1 (0) on the reactant (product) side of the dividing surface. The initial state along the proton displacement coordinate is assumed to be a Gaussian wave packet characterized by a width of about 3500 cm^{-1} (i.e., the approximate frequency of the O−H mode).

III. Results

Results are presented in five sections. First, section III.A presents results of ab initio quantum chemistry calculations associated with three P450 heme site models. Different parts in the hydrogen bond network, proximate to the O$_2$-binding cleft, are analyzed, and their role in the mechanism of proton transfer from W519 to the distal oxygen is investigated in terms of the minimum energy configurations in the *twice-reduced* dioxygen species. Section III.B presents results of ab initio calculations for the *reduced* oxyferrous species, and the effect of the second reduction in the proton-transfer mechanism is investigated. Section III.C presents ab initio results of the proton transfer in electronic states of different oxidation state or spin multiplicity. Section III.D presents ab initio results for the evolution of proton-transfer energy differences, ΔE, associated with 260 configurations of the thermally equilibrated solvated enzyme model. Section III.D also presents an analysis of the evolution of the geometries and their correlation with ΔE. Finally, section III.E presents results of full quantum dynamics simulations of proton transfer in a typical configuration of thermally equilibrated solvated enzyme. An ab initio proton-transfer energy profile is computed at the DFT level of theory, and the one-dimensional proton-transfer dynamics is simulated assuming a frozen configuration for all other degrees of freedom. This simple calculation gives an estimate of the characteristic times scales for proton transfer in a typical enzyme configuration and
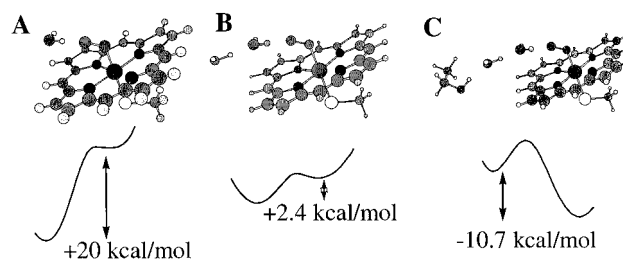
(46) Sadhukhan, S.; Munoz, D.; Adamo, C.; Scuseria, G. E. *Chem. Phys. Lett.* **1999**, *306*, 83.
(47) Feit, M.; Fleck, J.; Steiger, A. *J. Comput. Phys.* **1982**, *47*, 412.

Figure 3. Three different models systems investigated for analyzing the hydrogen bond network proximate to the O$_2$-binding cleft. (A) The system with only the reduced oxyferrous species and W519. (B) The system in (A) with W564. (C) The system in (B) with a Ser246 mimic.

presents a clear demonstration of the feasibility of proton tunneling through a typical proton-transfer energy barrier.

A. Proton-Transfer Energy Profiles. Figure 3 shows the ab initio proton-transfer energy profiles for three different models of the hydrogen bond network proximate to the O$_2$-binding cleft. The first model system includes the reduced oxyferrous heme species with the ligand O$_2$ and a water molecule that resembles W519. The second system includes all of the parts of the first system and an extra water molecule that resembles W564. Finally, the third system includes all of the parts of the second system and a HOCH$_2$CH$_3$ molecule that mimcs Ser246 in the P450eryF-binding site.

In the first system, the minimum energy complex corresponds to a "reactant" configuration where the O(W519)−H$_I$ distance is 0.98 Å, and the hydrogen bond length is 1.9 Å. It is found that there is no stable configuration for product in this minimal system, and therefore we conclude that a single water molecule cannot spontaneously donate a proton to the distal oxygen. Here we describe the calculation that shows this result. The "product" configuration is obtained by constraining the H$_I$−O$_{II}$ distance to 1.0 Å and fully optimizing the geometry with respect to all other degrees of freedom. Although a *constrained* "local minimum" is found for the product, the proton-transfer reaction is endothermic by 20 kcal/mol, and the "product" becomes unstable and spontaneously transforms back to the reactant geometry by releasing its geometry constraint.

A completely different proton-transfer energy profile is observed in the second system. Two well-stabilized local minima are found. These minima correspond to the reactant geometry, where O(W519)−H$_I$ = 1.00 Å and H$_I$−O$_{II}$ = 1.84 Å, and the product geometry, where O(W519)−H$_I$ = 1.60 Å and H$_I$−O$_{II}$ = 1.04 Å. Both of these minimum energy geometries are found without imposing any kind of geometry constraints. The proton-transfer energy difference is only slightly endothermic by 2.4 kcal/mol. The geometry of the product is found to be doubly degenerate, with two configurations that differ in the position of the proton between W519 and O(W564). Interconversion between the two degenerate products involves a nearly barrierless transformation (the barrier for the second proton transfer is smaller than the zero-point energy associated with this coordinate).

The starting geometry for the optimization of the third system is taken from the coordinates of the solvated P450eryF after thermal equilibration in the reduced oxyferrous heme form. Geometry optimization is performed by constraining the positions of the two carbons in the CH$_2$CH$_2$OH residue, the coordinates of the Fe atom, and the coordinates of one C atom in the porphyrin group. These constraints aim to preserve a
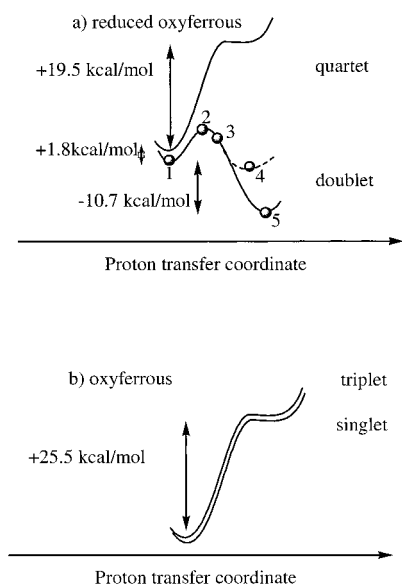
Figure 4. Examination of the proton-transfer reactant and product energies on (a) the lowest doublet and quartet electronic states of the reduced oxyferrous species, and (b) the singlet and triplet oxyferrous species (i.e., prior to the second reduction step). Panel a for the doublet surface also displays the reaction coordinate points. The reaction coordinate geometries and relative energies are given in Table 1.

Table 1. Geometries and Energies Associated with Points 1−5 along the Minimum Energy Path for Proton Transfer from W519 to O_{II} (See Figure 2)

	point label				
	1	2	3	4	5
$H_{III}-O_{564}$	2.03	1.96	1.95	1.80	1.50
$O_{564}-H_{II}$	1.00	1.02	1.05	1.05^a	1.69
$H_{II}-O_{519}$	1.79	1.66	1.56	1.47	1.03
$O_{519}-H_{I}$	1.00	1.19	1.35	1.97^a	2.30
$H_{I}-O_{II}$	1.85	1.25^a	1.20^a	1.00	0.98
energy (kcal/mol)	0.00	6.80	5.90	−0.20	−10.7

^{a} Distance has been constrained during geometry optimization. All distances in this table are expressed in angstroms.

configuration that is similar to the geometry found in the crystallographic structure, even in the absence of the protein environment.

The proton-transfer product in the third model system is found to be 10.7 kcal/mol more stable than the reactant. The product minimum energy geometry involves a double proton transfer within the H-bond network and is 10 kcal/mol more stable than a constrained product, where only H_I is transferred.

These results provide the first direct evidence that a locally ordered hydrogen bond network in the P450eryF-binding cleft can drastically change the proton-transfer energy profile and facilitate proton translocation from W519 to the distal oxygen.

B. Reaction Coordinate for Proton Transfer. Figure 4 shows the proton-transfer energy profile, as a function of the $O(W519)-H_I$ distance, for the third model system of section III.A. Panel a shows the ab initio energy points for five different configurations of the system. The geometries and energy values associated with these five configurations are presented in Table 1. These configurations are obtained as follows. Point 1 corresponds to the optimized minimum energy geometry in the reactant configuration ($H_I-O_{II} = 1.85$ Å). Starting from point 1, the configurations of points 2 and 3 are generated by optimizing the geometry of the system subject to the constraint

of $H_I-O_{II} = 1.25$ and 1.20 Å, respectively. The geometries of points 2 and 3 show that, during the first proton transfer, the $O_{564}-H_{II}$ bond length remains practically unchanged, and that the barrier for the first proton transfer along the minimum energy path (MEP) is approximately 7 kcal/mol. The geometry changes associated with points 2 and 3 show that the reaction coordinate involves some reorganization, where W519 gets closer to W564.

The configuration of point 4 is obtained by starting from the configuration associated with point 3, and optimizing the geometry of the system subject to the constraint of $O_{564}-H_{II} = 1.05$ Å. At point 4, the first proton has been completely translocated, and the energy of the system is approximately the energy of the reactants (point 1). The configuration of point 5 is obtained simply by releasing the constraint on the $O_{564}-H_{II}$ bond. This allows the second proton translocation to occur, a barrierless process that further stabilizes the system by 10.5 kcal/mol.

The analysis of the energy and geometry changes along the minimum energy path describes a detailed mechanism for protonation of the distal oxygen, where the hydrogen bond network proximate to the O_2-binding cleft plays a crucial functional role. According to this sequential double proton transfer, W519 plays the role of both a proton donor and a proton acceptor in a Grotthuss-like mechanism. The results presented in this section indicate that the limiting step corresponds to the first proton transfer, from W519 to O_{II}. Therefore, the analysis of the ensemble of thermally equilibrated configurations will be focused on this fundamental step.

It is important to emphasize that significant changes in the coordinates of the heavy atoms in the hydrogen bond network occur with variation of the H_I-O_{II} distance. Therefore, the MEP does not lie simply along a H_I-O_{II} proton-transfer coordinate. The large curvature in the overall reaction coordinate indicates the importance of exploring tunneling paths. These paths describe shorter displacements that might deviate significantly from the MEP. Once again, we note that the reaction coordinate involves displacements of water molecules away from the newly formed OOH ligand. These displacements reinforce the hydrogen bond between between Ser246 and W564 and facilitate the reorganization of the OOH ligand to favor a second proton translocation.

C. Proton Transfer in Electronic States of Different Oxidation State or Spin Multiplicity. All calculations discussed up to this point correspond to the reduced oxyferrous species, i.e., considering the protonation of the distal oxygen after the second reduction of the system. The ground state for the twice-reduced species is a doublet state. However, the reactant quartet is found to lie just a few kilocalories per mole above the doublet state. Panel a of Figure 4 shows the comparison of proton-transfer energy profiles for the doublet state of the reduced oxyferrous species and the quartet spin electronic state for the same oxidation state. Contrary to protonation in the doublet state, where the reaction is exothermic by 10.5 kcal/mol, protonation in the quartet state is found to be endothermic by 19.5 kcal/mol. We, therefore, rule out the possibility of relaxation through proton transfer in the quartet state. Figure 4, panel b, shows proton-transfer energy profiles in the singlet and triplet states of the oxyferrous species, i.e., before the second reduction has occurred. These results provide the first clear theoretical evidence that the second reduction is
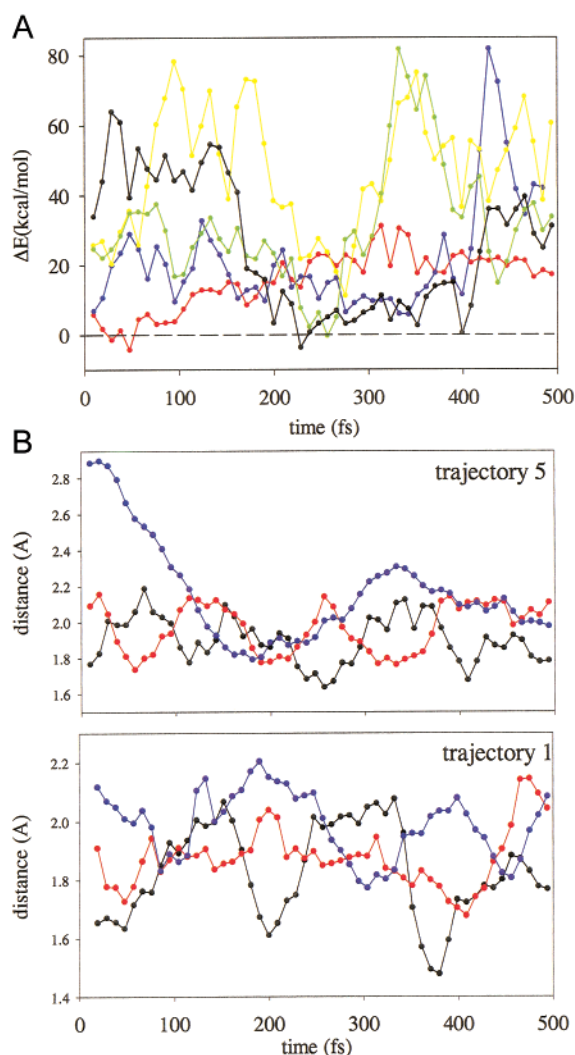
Figure 5. Energetic (DFT)/geometric analysis of the MD-DFT trajectories. (A) The single proton-transfer DFT energy difference ($E_{\text{prod.}} - E_{\text{react.}}$) for nuclear configurations sampled from molecular dynamics simulations. Positive values correspond to endothermic proton transfer, while negative values indicate exothermic reaction conditions. Of the five trajectories shown in this figure, three of them present negative energy differences between 20 and 60 fs (trajectory 1 in red), between 240 and 260 fs (trajectory 4 in green), and between 220 and 240 fs (trajectory 5 in black). (B) The evolution of hydrogen bond lengths, in angstroms, for trajectories 1 and 5 (red and black in panel A, respectively). In black, H-bond 1, H_I-O_{II}; in red, H-bond 2, $H_{II}-O_{519}$; in blue, H-bond 3, $H_{III}-O_{564}$, as introduced in Figure 2.

necessary and responsible for generating the electric field that triggers the proton-transfer mechanism described in section III.B.

D. Full Dimensional Study. Figure 5, panel A, shows the time evolution of instantaneous proton-transfer energy differences, $\Delta E(t) = E_{\text{prod.}}(t) - E_{\text{react.}}(t)$, for 500 fs of dynamics of the solvated enzyme in its reduced oxyferrous bound heme form. Here, $E_{\text{react.}}$ corresponds to the energy of the thermally equilibrated system at time t, and $E_{\text{prod.}}$ is the energy of the product generated according to the sudden proton-transfer approximation from W519 to the distal oxygen O_{II}— i.e., the configuration of the product is identical to the configuration of the reactant, except for the coordinate of the proton being transferred. Figure 5 shows results for five statistically independent trajectories of the system. The ab initio energy difference, ΔE, is estimated by using the third model system of section III.A, parametrized according to the instantaneous configuration of the solvated

enzyme. The model includes the P450 heme site with the ligand O_2, a water molecule with the coordinates of W519, a second water molecule parametrized by the coordinates of W564, and a $HOCH_2CH_3$ molecule where the coordinates of the two C atoms and the coordinates of the O and H atoms in the hydroxyl group correspond to the coordinates of the corresponding atoms in Ser246.

Figure 5 shows that the initial protonation of the distal oxygen becomes energetically accessible within a time scale of 500 fs. These results show not only that the initial protonation is feasible for certain nuclear configurations, but also that such configurations are favorable in the full protein environment. Our results indicate that, in less than 500 fs, thermal motion in the full protein environment brings the reactant into configurations that are favorable for proton transfer. This phenomenon is observed in more than 50% of the trajectories. Note that $\Delta E \approx 0$ between 30 and 60 fs (trajectory 1), between 240 and 260 fs (trajectory 4), and between 230 and 260 fs (trajectory 5). It is important to note that these favorable conditions are met even in the absence of excess protons in the system.

Figure 5, panel B, shows the temporal evolution of the three H-bonds for two of the five trajectories analyzed in panel A. The three hydrogen bond lengths displayed in panel B correspond to H-bond 1, H_I-O_{II} (black points); H-bond 2, $H_{II}-O(W519)$ (red points); and H-bond 3, $H_{III}-O(W564)$ (blue points).

The first feature to note is that the average bond length for the three successive H-bonds increases as they are farther away from the O_2 heme-ligand. This result is consistent with the effect of a localized excess electron density in the heme-bound oxygen of the reduced oxyferrous species.[15,48]

The second important aspect to note is that there is a correlation between optimal conditions for proton transfer (i.e., $\Delta E \approx 0$) and a value for the H_I-O_{II} bond length of about 1.7 Å. This is observed at 30−60 fs for trajectory 1, and at 220−240 fs for trajectory 5. These optimal conditions, however, are not restricted to one specific bond length (e.g., the H_I-O_{II} bond length) but involve other important geometrical aspects analyzed in Figure 6.

Figure 6 shows the evolution of the $O(W519)-O_{II}-O_I$ angle for trajectories 1 and 5. This angle precisely describes the orientation of W519 relative to the bound dioxygen ligand. The value of this angle in the fully optimized geometry for the reduced system is 115°. This value is approximately reached in both trajectories 1 and 5, at the times when $\Delta E \approx 0$. This critical orientation of *W*519 is also manifested at approximately 200 and 350 fs in trajectory 1, where the W519 lies above the optimal H-bond alignment (i.e., the $O(W519)-O_{II}-O_I$ angle > 115°). Proton transfer is, therefore, substantially endothermic, even when the system has an optimum H_I-O_{II} bond length of approximately 1.7 Å. The reason for this is that the orientation of W519 determines how effective is the overlap between the proton acceptor (i.e., the orbital with a lone pair of valence electrons in O_{II}) and the HO bond in W519.

Figure 6 also shows the evolution of the $O_{II}O_IFeN$ dihedral angle (see Figure 2). This angle defines the orientation of the O_2 ligand with respect to the heme plane. This orientation ultimately determines the overlap between the O_{II} lone pair and

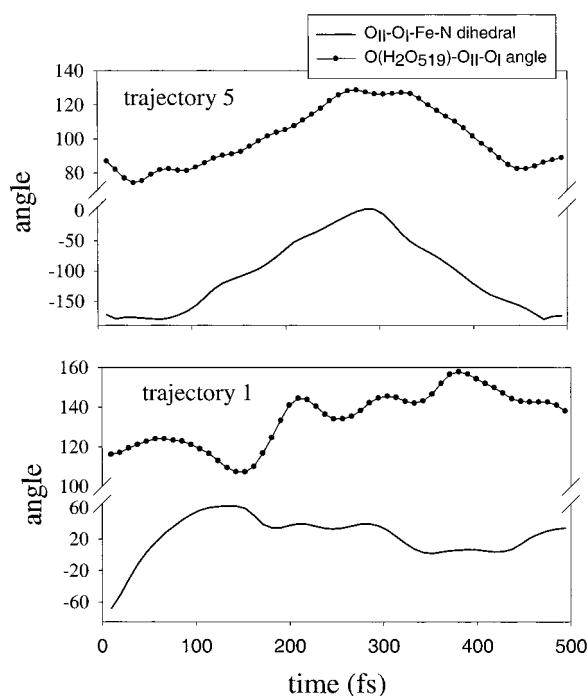(48) Harris, D.; Loew, G.; Waskell, L. *J. Am. Chem. Soc.* **1998**, *120*, 4308.

Figure 6. Evolution of the O(W519)$-$O$_{II}$$-O_I$ angle (line points) and the O$_{II}$$-O_I$$-Fe-$HEMEplane (line) dihedral angle for the first and fifth trajectories during 500 fs of dynamics. The values for these angles in the single proton-transfer product (point 4 in Figure 4) are 116° and −79°, respectively, in good agreement with the values observed in the MD simulations at times when $\Delta E \approx 0$: 20−60 fs (trajectory 1) and 220−260 and 400 fs (trajectory 5).

the OH bond. Values in the −50° to −90° range are characteristic of reactant geometries that are close to its value in the fully optimized geometry configuration (i.e., −79°). Figure 6 shows that the O$_{II}$O$_I$FeN dihedral angles are in the −50° to −90° range when $\Delta E \approx 0$.[49]

In summary, the detailed examination of the geometries that are strongly correlated with optimum conditions for proton transfer (i.e., $\Delta E \approx 0$) revealed a common pattern, namely that the proton-transfer probability is highly correlated with geometric features that define maximum stability in the hydrogen bond network. Our results clearly show that thermal fluctuations that move the system away from this optimal configuration are strongly correlated with changes in the proton-transfer efficiency. Our calculations also show that the proton-transfer energy *difference* is rough in the scale of many kT (see Figure 5), and therefore proton transfer is mostly determined by the time scale associated with the reorganization of the hydrogen bond network. The reorganization process generates optimal configurations that usually survive for about 20−30 fs. This lifetime is sufficiently long as to allow complete proton translocation. The proton translocation dynamics is discussed in section III.E.

E. Quantitative Proton Transfer. Figure 7 shows the time-dependent survival probability, $P(t)$, for proton transfer in a representative specific configuration. It is assumed that the

(49) Ab initio calculations of the heme$-$O$_2$ dihedral angle were performed to verify the force field parametrization of this coordinate. The energies obtained with the force field parameters for the bound O$_2$ rotational angle were found to be in semiquantitative agreement with the ab initio results. These calculations showed very small energy changes as a function of the heme$-$O$_2$ dihedral angle, which allowed for optimization of the O$_2$ orientation with respect to the hydrogen bond network.

Table 2. Evolution of Proton-Transfer Energy Barriers for Three Representative Trajectories (Energies Are Expressed in kcal/mol)

trajectory 1		trajectory 2		trajectory 3	
time (fs)	energy	time (fs)	energy	time (fs)	energy
9.5	7.1	218.5	19.0	209.0	12.2
19.0	0.2	228.0	9.8	218.5	9.0
28.5	0.0	237.5	4.7	228.9	0.0
38.0	3.1	247.0	3.9	237.5	0.0
47.5	0.6	256.5	2.2	247.0	0.3
57.0	2.5	266.0	6.9	256.5	1.5
66.5	3.9	275.5	24.0	265.0	1.3
76.0	3.4			275.5	2.5
85.5	5.9			285.0	6.2
95.0	7.4			294.5	9.6
104.5	12.2			304.0	14.0
114.0	14.0			313.5	8.0

system is prepared with that specific nuclear configuration at time 0, and that the reorganization of the remaining degrees of freedom is much slower than proton motion. The nuclear configuration corresponds to the configuration of the system in the trajectory 5 at $t = 342$ fs (see Figure 5). Figure 7 also shows the instantaneous proton-transfer energy profile and the ab initio DFT energy points computed for this specific configuration. The zero-point energy is indicated in the reactant side to show that, for this specific nuclear configuration, proton transfer is a classically forbidden process.

The time-dependent survival probability associated with this specific configuration shows that the relaxation process is completed with 10−15 fs of dynamics. The relaxation dynamics gives rise to a ∼10% population decay, even when proton transfer is dominated by tunneling through a 10 kcal/mol energy barrier.

Table 2 shows the evolution of proton-transfer energies barriers for trajectories 1, 4, and 5 (see Figure 5).

Table 2 shows that optimal configurations (i.e., $\Delta E \approx 0$) correlate with barrierless proton-transfer energy profiles. Slightly endothermic reactions have energy barriers in the 3−10 kcal/mol energy range. The difference in time scales associated with proton translocation (completed in less that 10 fs), and the time scale of reorganization modes in the hydrogen bond network (<300 cm^{-1}), allow us to simulate the actual proton translocation as a relaxation process though a constant one-dimensional proton-transfer energy profile. This approximation is justified by the data in Table 2, where it is shown that significant changes in energy barriers usually involve time scales that are >20 fs.

IV. Summary and Conclusions

In this paper, we have shown that the transient pathway of cytochrome P450eryF, from the oxyferrous species to the catalytically active ferryl oxygen species (compound I), involves an ultrafast proton transfer from the crystallographic water molecule W519 to the distal oxygen bound to the heme group, and a subsequent proton-transfer event from W519 to W564 with a subpicosecond time scale. We have shown that the rate-determining step in this double proton-transfer mechanism is the initial proton transfer from W519 to the distal oxygen. This initial proton translocation produces a reorganization of the hydrogen bond network that leads to a spontaneous and exothermic second proton transfer. This second proton transfer stabilizes the initial translocation by approximately 10 kcal/mol.
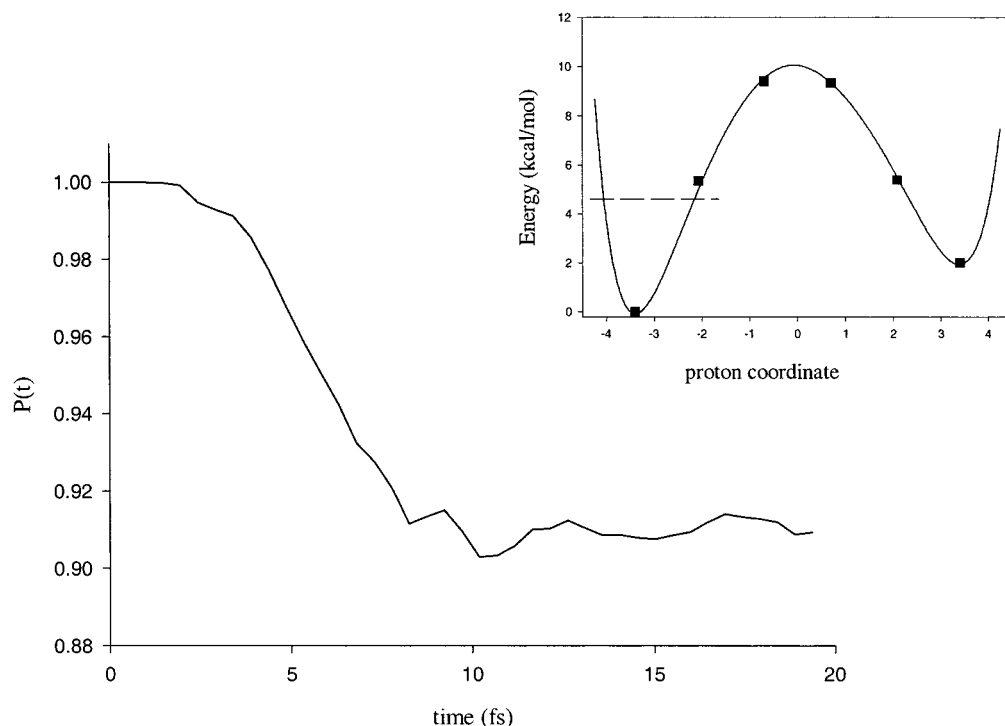
Figure 7. Quantum dynamics simulation of proton-transfer dynamics through a ~10 kcal/mol energy barrier.

The DFT calculations of the proton-transfer reaction in the oxyferrous and reduced oxyferrous forms have indicated that the second reduction and the proton-transfer reactions are mechanistically coupled. We have found clear evidence that the second reduction drastically changes the instantaneous proton-transfer energy profiles and triggers a sequential double-proton mechanism in the hydrogen bond network that is proximate to the O_2-binding cleft. This involves a Grotthuss-like mechanism where W519 plays the role of a proton donor in the first step and a proton acceptor in the second step.

We have shown that the conditions under which direct protonation of the heme bound distal oxygen occurs, via proton transfer from W519, correspond to geometrical features associated with configurations where the hydrogen bond network reaches its maximum stability. These features are commonly found within 500 fs of dynamics and include optimal hydrogen bond bond lengths and optimal orientations of both the ligand and the water molecules near the O_2-binding cleft. These conditions typically coincide with optimal alignment of proton donor–acceptor orbitals.

We have shown that our results are consistent with isotopically enriched oxygen experiments,[16–18] where it was found that the "distal" oxygen is involved in the concurrent formation of water after the second reduction. We have also shown that our results are consistent with mutation experiments that have shown a significant correlation between the occupancy and/or mobility of the W519 and the reduction in enzymatic turnover for the system.[42,43] The considerable modulation of activation energies with the configuration of the hydrogen bond network makes it clear that mutational changes that affect the structure or dynamics of this hydrogen bond network can produce large and immediate effects on the corresponding proton-transfer dynamics.

We have shown that the simplest approach for finding optimal configurations for proton transfer, and analyzing the proton-transfer relaxation, can be justified in terms of the comparison of time scales associated with the lifetime of optimal configurations and the proton translocation dynamics. Our results have illustrated the potential of this simple approach that involves a combination of DFT single-point calculations and standard molecular mechanics techniques for gaining insight with respect to proton-transfer dynamics in biomolecules. This hybrid method, however, is only the first step in our final goal of implementing rigorous semiclassical methods to investigate quantum reaction dynamics in complex biological systems.